

## Early optical observations of GRBs by the TAROT telescopes: period 2001-2008

A. Klotz

*Observatoire de Haute Provence (CNRS-OAMP), 04870 Saint Michel l'Observatoire, France  
Centre d'Etude Spatiale des Rayonnements, 9 avenue colonel Roche, 31028 Toulouse Cedex 4, France*

klotz@cesr.fr

and

M. Boër

*Observatoire de Haute Provence (CNRS-OAMP), 04870 Saint Michel l'Observatoire, France*

michel.boer@oamp.fr

and

J.L. Atteia

*Observatoire Midi Pyrénées, LATT (UPS-CNRS), Université de Toulouse, 31400 Toulouse, France*

atteia@ast.obs-mip.fr

and

B. Gendre

*Laboratoire Astronomique de Marseille, LAM (UP-CNRS), Université de Provence, 38, rue Frédéric  
Joliot-Curie, 13388 Marseille cedex 13, France*

bruce.gendre@oamp.fr

### ABSTRACT

The TAROT telescopes (*Télescopes à Action Rapide pour les Objets Transitoires*) are two robotic observatories designed to observe the prompt optical emission counterpart and the early afterglow of gamma ray bursts (GRBs). We present data acquired between 2001 and 2008 and discuss the properties of the optical emission of GRBs, noting various interesting results. The optical emission observed during the prompt GRB phase is rarely very bright: we estimate that 5% to 20% of GRBs exhibit a bright optical flash ( $R < 14$ ) during the prompt gamma-ray emission, and that more than 50% of the GRBs have an optical emission fainter than  $R = 15.5$  when the gamma-ray emission is active. We study the apparent optical brightness distribution of GRBs at 1000 sec showing that our observations confirm the distribution derived by other groups. The combination of these results with those obtained by other rapid slewing telescopes allows us to better characterize the early optical emission of GRBs and to emphasize the importance of very early multi-wavelength GRB studies for the understanding of the physics of the ejecta.

*Subject headings:* telescope: general — GRBs: individual ( GRB 010213, GRB 020531, GRB 030115, GRB 030324, GRB 030329, GRB 030501, GRB 040916, GRB 041006, GRB 041218, GRB 041219A, GRB 050209, GRB 050306, GRB 050408, GRB 050416, GRB 050504, GRB 050505, GRB 050520, GRB 050525A, GRB 050730, GRB 050803, GRB 050824, GRB 050904, GRB 051211A, GRB 051211B, GRB 051221B, GRB 060111A, GRB 060111B, GRB 060124, GRB 060512, GRB 060515, GRB 060814, GRB 060904A, GRB 060904B, GRB 060919, GRB 061019, GRB 061027, GRB 061028, GRB 061110B, GRB 061217, GRB 061218, GRB 061222B, GRB 070103, GRB 070227, GRB 070330, GRB 070411, GRB 070412, GRB 070420, GRB 070508, GRB 070521, GRB 070621, GRB 070628, GRB 070913, GRB 070920A, GRB 070920B, GRB 071010A, GRB 071101, GRB 071109, GRB 071112B, GRB 071112C, GRB 080129, GRB 080207, GRB 080210, GRB 080315, GRB 080330, GRB 080413A, GRB 080430, GRB 080516, GRB 080603B, GRB 080903 ) —

## 1. Introduction

The discovery of Gamma-Ray Burst (GRB) optical afterglows in 1997 (van Paradijs et al. 1997) and the creation of the Internet message distribution service by BACODINE and the Gamma-ray burst Coordinate Network (GCN, Barthelmy et al. 1998) gave the impulse to look for the *prompt* optical emission of GRBs<sup>1</sup>. The first detection of the prompt optical emission from a GRB was performed by ROTSE-I on GRB 990123 (Akerlof et al. 1999). The exceptionally bright optical emission of GRB 990123 ( $V \sim 9$ ) was uncorrelated with the gamma-ray light-curve. After 2001, the operation of satellites providing fast GRB localizations (HETE-2, INTEGRAL, *Swift*, AGILE, *Fermi*) have allowed the detection of some GRBs with *bright* optical emission during their gamma activity (typically  $R < 13$ ). These bursts usually follow a behavior similar to GRB 990123, with a single bright peak at optical wavelengths (e.g. GRB 060111B Klotz et al. 2006).

On the other hand, using the trigger delivered by the *Swift* satellite (Gehrels et al. 2004), Vestrand et al. (2006) detected a faint optical emission correlated with the gamma-ray light-curve in GRB 050820A. Though there are few bursts that are well observed at optical wavelengths during the gamma-ray emission, it seems that GRB 990123 and GRB 050820A are prototypes of two categories of GRBs: *i*) those with bright optical transients uncorrelated with the gamma-ray activity often interpreted as the result of reverse shocks (Jin & Fan 2007), and *ii*) those with faint optical emission correlated with the gamma-ray light-curve often interpreted as the low energy tail of the high-energy emission (Genet et al. 2007).

Understanding the multi-wavelength emission of GRBs during the prompt phase is very important, as it provides direct insight into the composition of the ejecta and its physical conditions. In the optical such studies require the combination

---

<sup>1</sup>Throughout this paper the term 'prompt emission' refers to the photons detected when the GRB is *active* (or in the *prompt* phase). This *prompt* phase is arbitrarily defined as starting with the trigger and ending after  $T_{90}$  seconds, where  $T_{90}$  is the time during which 90% of the burst photons are detected (from 5% to 95% of the cumulated photon fluence).

of GRB satellites providing fast alerts and rapid slewing telescopes on the ground. The launch of *Swift* has increased by an order of magnitude the number of alerts sent to ground observatories, allowing small robotic telescopes to contribute actively to the study of the prompt GRB emission at optical wavelength. This is in particular the case of the two TAROT robotic telescopes, which are designed to observe the optical emission during the first seconds following a GRB alert (Klotz et al. 2009). They are able to slew very rapidly to any sky location above their horizon upon receipt of GCN notices.

This paper is devoted to the analysis of the GRB observations made by TAROT during the period 2001-2008. Depending on the burst, observations started either during the prompt emission or the afterglow. Section 2 summarizes the main technical characteristics of the two robotic TAROT observatories. Section 3 describes the acquisition strategies and image processing methods. Section 4 is devoted to the analysis of the prompt optical emission. From our data we derive the apparent optical brightness distribution of GRBs at 1000 sec in Section 5. In Section 6 we discuss how the afterglows seen by TAROT can be used for cosmological studies.

## 2. TAROT observatories

The TAROT telescopes were designed in 1995, two years before the first optical detection of a GRB. At this epoch, the size of the error boxes provided by the CGRO-BATSE experiment (Fishman et al. 1992) was about  $5^\circ \times 5^\circ$ . As a consequence, the field of view (hereafter FoV) of TAROT was designed to be large enough to cover as much as possible of the BATSE error boxes. Two telescopes were planned: one in France (operating since 1998) at the Calern observatory (Observatoire de la Côte d'Azur, CNRS), the second in Chile (active since 2006) at the La Silla European Southern Observatory. In order to reach the position of the GRB provided by the GCN as quickly as possible, the mount can move as fast as  $50^\circ \text{sec}^{-1}$ . Primary mirrors are 25 cm in diameter and 85 cm in focal length. These observatories are fully autonomous and robotized (scheduling, acquisition and data management). A detailed description of the telescopes can be

found in Klotz et al. (2009).

From 1998 to 2000, the detector was an APOGEE camera based on a Kaf-1300 CCD chip that covered only  $1.3^\circ \times 1.1^\circ$ . The slewing strategy was to make a mosaic of 25 images in order to cover most of the BATSE FoV. Since the exposure time was 30 sec and the readout time was 30 sec, it implied that the complete survey lasted about 25 minutes for a limiting magnitude of 14. Twenty-one BATSE triggered GRBs were observed by TAROT during that period (Boër et al. 2001). Due to the large delays between alert and observations and the poor limiting magnitude, we do not include these events in the present analysis.

After 2001, the HETE (Ricker et al. 2001) error boxes were smaller than  $\simeq 20'$ . They fitted easily in one  $1.9^\circ \times 1.9^\circ$  image made by the new custom camera based on a TI-7899 chip from Thomson, allowing rapid slewing to the source location and an earlier observation of the optical emission. In 2003, this camera was replaced by an ANDOR 436, based on a Marconi-4240 back illuminated CCD. The FoV remains essentially the same:  $1.86^\circ \times 1.86^\circ$ . Since 2003, TAROT observed GRBs triggered by INTEGRAL and by *Swift* (Gehrels et al. 2004) with error boxes smaller than  $3'$ .

The last significant evolution of the program was the installation of TAROT ‘La Silla’ in Chile whose first light occurred in 2006 with the same ANDOR 436 camera, and characteristics similar to TAROT ‘Calern’.

### 3. GRB observations with TAROT

Since December 2005 we have adopted a strategy resulting in the acquisition of a series of exposures that optimizes the signal to noise ratio (SNR) and the time resolution. The first image of this series is an unfiltered 60-sec exposure taken with a slight drift along the diurnal motion. This strategy results in a trailed image of the afterglow with no dead-time. Such a trailed image will readily display any rapid variations of the optical emission. The drift is calibrated to get  $6 \text{ sec pixel}^{-1}$ . For the brightest afterglows, this provides a time-resolved light-curve with a temporal resolution of several seconds (typically 5–10). After the trailed image, five 30-sec unfiltered exposures are taken with no drift. This then completes the first series of images. After this series, four series of three

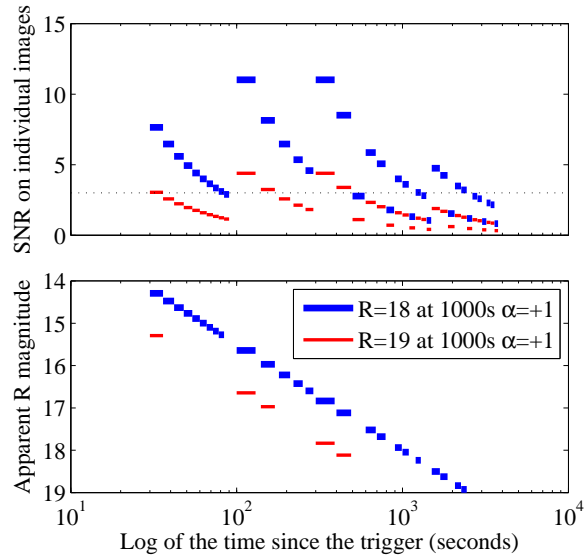


Fig. 1.— The observing strategy is illustrated by two simulated afterglows: R=18 at 1000 sec with  $\alpha = +1$  ( $f(t) \propto t^{-\alpha}$ , thick blue lines in the online edition), and R=19 at 1000 sec with  $\alpha = +1$  (thin red lines in the online edition) Top panel: Signal to noise ratio (SNR) as a function of elapsed time since trigger considering the actual series of exposure performed by TAROT (see section 3). Bottom panel: the corresponding time resolved light-curves from individual images. For the fainter GRB, the final light-curve is made by co-adding individual images in order to increase the detectivity.

90-sec long images are made, the first two images of each series are unfiltered and the third is taken with an R filter. When possible, 180-sec exposures are taken with the same filter sequence until 4 hours after the trigger. The resulting SNR and the light-curve are presented for two simulated cases in Figure 1. A late follow-up is performed, acquiring a series of VRI 180-sec images every 15 minutes until the end of the night.

Tables 1 and 2 summarize the TAROT optical observations of 72 GRBs that were observed between 2001 and 2008. During that period, twenty optical transients were detected. For eleven of them there is more than one detection available, allowing the measure of the temporal decay index. When the gamma-ray emission is still active, four-

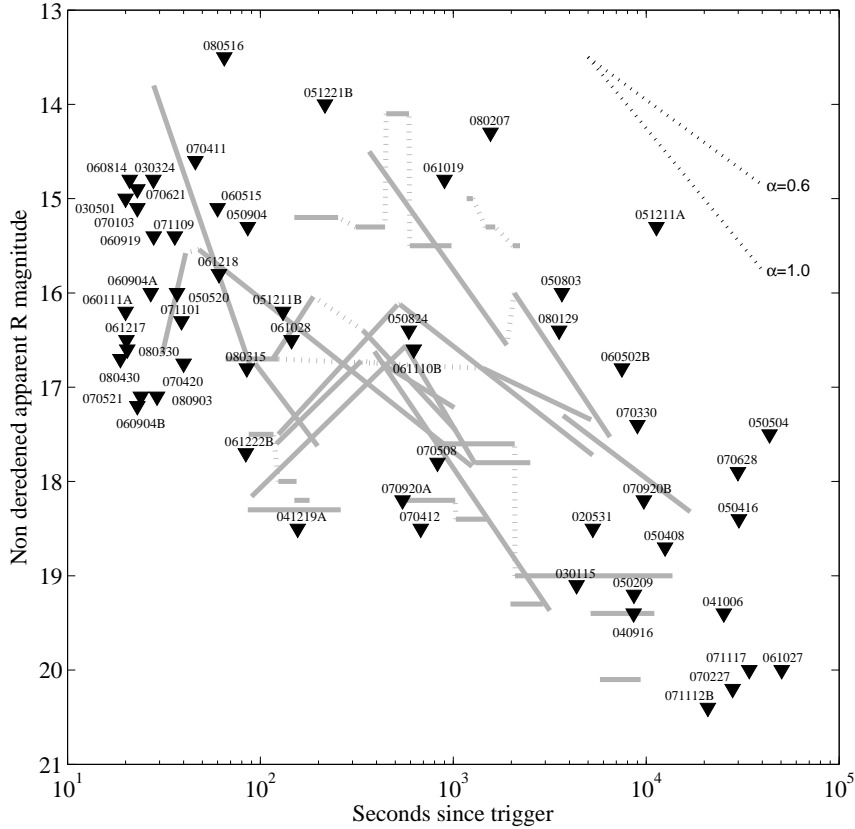


Fig. 2.— TAROT observations of the early optical emission from GRBs: the triangles represent upper limits for the first time bin and the thick gray lines are the light-curves of detected sources. Upper limits are identified with the name of the GRB, for light-curve identification, see Fig 3. The dotted lines on the upper right corner illustrate two typical afterglow decay slopes. The data are from Tables 1 and 2 of this paper.

teen GRBs were observed and 3 of them showed an optical emission detected by TAROT.

The majority of data displayed in Tables 1 and 2 have been published in GCN Circulars and various papers (listed in column 6 of each table). We correct here some errors published in the GCN circulars for GRB 050520 and GRB 050730, due to bad dates and poor quality calibration, now refined. The limiting magnitude of the first image of GRB 030501 was measured during the prompt emission. GRB 060124 was embedded in a bright star. The optical counterpart was extracted by image difference that leads to a lower limit. We also performed a full analysis of the images of GRBs for which TAROT started observing very late: GRB 050408, GRB 050416, GRB 050504

and GRB 050824. These results are summarized in Figure 2 which displays the detections and one upper limit for those GRBs which have not been detected. Figure 3 displays all the detected optical emissions. On these figures, we have plotted the observed magnitudes, without any correction for the galactic extinction or for the cosmological effects.

The afterglow decay, which can start during the prompt event, is usually described by a power-law of index  $\alpha$  ( $f(t) \propto t^{-\alpha}$ , where  $f(t)$  is the observed flux). According to (Zeh et al. 2006),  $\alpha$  lies between 0.5 and 1.7 with a median value of 1.0. Additional features can make the afterglow decay more complex. Many afterglows detected by TAROT exhibit an increase in brightness

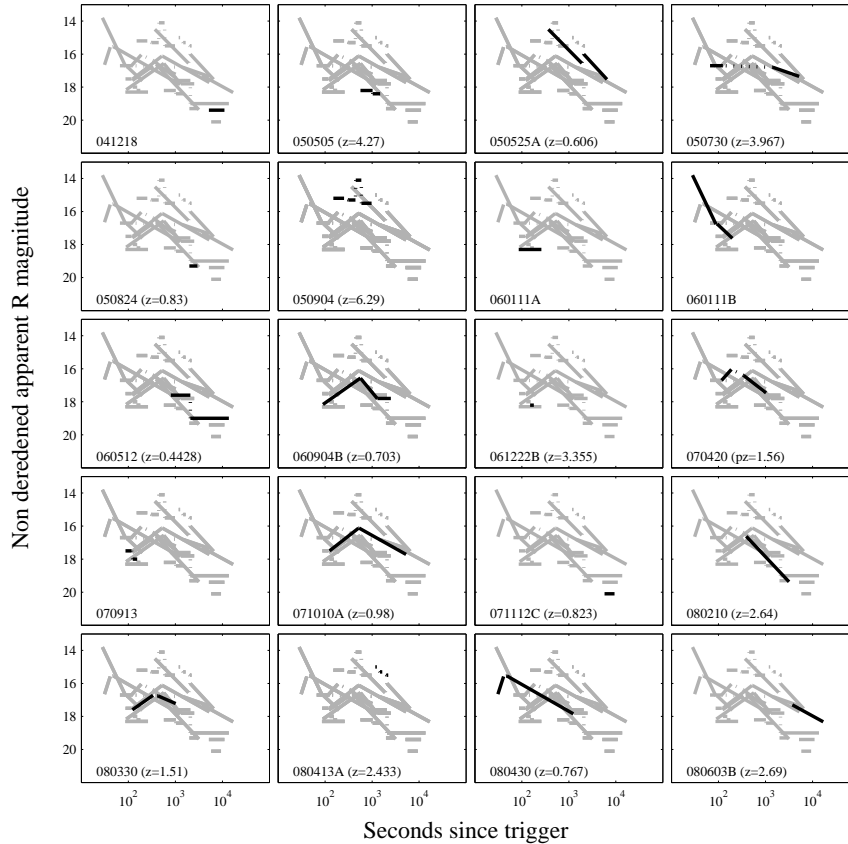


Fig. 3.— TAROT detections of GRB afterglows. Twenty GRB afterglows detected by TAROT are shown for comparison, one per box. The black curves correspond to the GRB indicated at the bottom of the box. Gray lines are the other GRBs detected by TAROT. 16 GRBs have redshifts – indicated at the bottom of their respective boxes above. (Note that the ‘pz’ for GRB 070420 stands for ‘pseudo-redshift’.)

until a few hundreds of seconds (GRB 050904, GRB 060904B, GRB 070420, GRB 071010A, GRB 080330, GRB 080430). In all cases, the decay regime of the afterglow,  $t^{-\alpha}$ , is well established after 600 sec. In the cases of GRB 050525A and GRB 060904B, the light-curves show a plateau or a rebrightening near  $2 \times 10^3$  sec in the rest frame.

#### 4. Optical emission during gamma-ray activity

Because the TAROT slewing time is about 5 sec, and the *Swift*-GCN notification time takes about 20 sec, only the longest GRBs can be studied during their prompt emission. Figure 4 shows the histogram of the delay between the trigger and the start of the first observation. The black bars

represent events that were observed by TAROT before the end of the prompt emission, there are 14 such events. This figure shows that 90% of the bursts (10/11) are still in the prompt phase after 40 sec and that no GRB afterglow is observed during the prompt emission after a delay of about 200 sec.

Figure 5 displays the measurements done by TAROT during the prompt phase of 12 GRBs. Though 14 events were observed by the TAROTs during the prompt emission, only 12 of them appear in Figure 5 because we have eliminated two bursts. GRB 030501 was observed through a high extinction region of the Galaxy, preventing us from giving meaningful constraints on the brightness of its afterglow and GRB 050306 has

a poor upper magnitude limit due to a low elevation and the presence of haze. Figure 5 shows that GRB 060111B was the brightest of the detected emissions, and it exhibits a fast decay. The rise of the afterglows of GRB 050904 and GRB 060904B started before the end of the gamma-ray activity but no emission was detected during the first trailed exposure. This figure also shows that more than 50% of the GRBs are fainter than  $R = 15.5$  during the prompt phase. Optically bright GRBs with a rapid decay phase, like GRB 060111B (or GRB 990123) seem to be rare: at most 5 to 20% of the bursts.

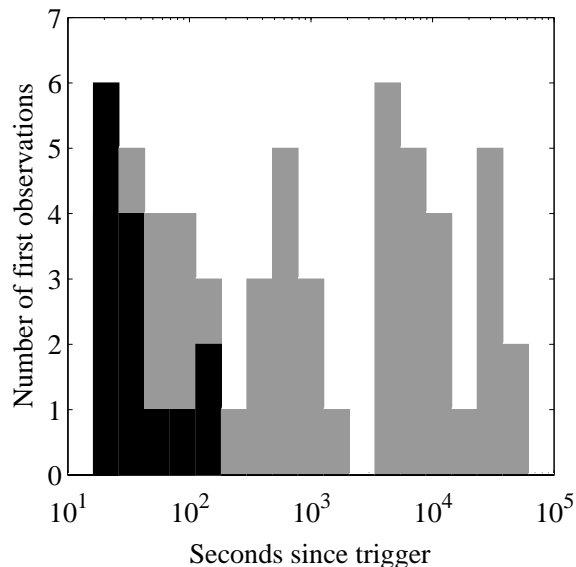


Fig. 4.— Histogram of the observation delays between the trigger and the start of the first TAROT exposure. Black bars represent exposures which started while the gamma-ray emission was still active.

## 5. Afterglow brightness distribution

Several authors have discussed the afterglow apparent brightness distribution (*e.g.* Berger et al. 2005; Fiore et al. 2006). The first problem is to define the brightness since the source luminosity decreases rapidly. Here we follow the approach of Akerlof & Swan (2007, hereafter AS07), and we define the reference brightness as the apparent  $R$  magnitude 1000sec after the GRB trigger, dereddened from the galactic extinction. This enables

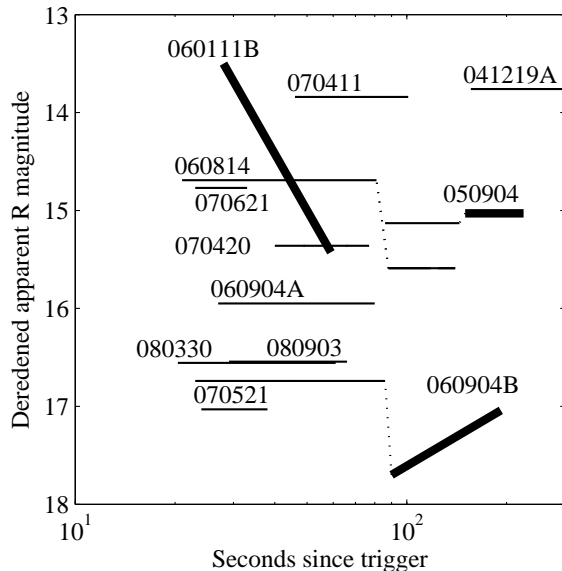


Fig. 5.— Plot of TAROT measurements performed while the GRB was still active. Thick lines are detections and horizontal thin lines represent upper limits. The magnitudes are dereddened from the galactic extinction. GRB 030501 and GRB 050306 are not shown on this plot because of the poor constraints on the brightness of their optical afterglows resulting from a high galactic absorption (GRB 030501) and/or a poor sensitivity limit (GRB 050306).

us to alleviate somewhat the biases introduced by the erratic behaviour of the optical emission which is sometimes observed during the first hundreds of seconds after the trigger.

When TAROT observations stop before 1000sec we extrapolate the light-curve to 1000sec using a temporal index  $\alpha = +1.0$ . For observations starting between 1000 and 2000sec, we extrapolate the light-curve backward with the same index. We do not include GRBs for which the first exposure started after 2000sec since the extrapolation may lead to additional biases. In total we have 45 events with 12 positive measurements and 33 upper limits. This is much less than the 109 GRBs with 43 positive detections quoted in AS07. However, AS07 mixes data from 29 different telescopes from 6 to 820 cm aperture and  $\sim 40\%$  of data come from the UVOT onboard the *Swift* satellite, which may introduce various biases. In particular, un-

like ground telescopes the UVOT cannot observe in the R band, requiring a k-correction based on the optical spectral index and the host extinction which is usually poorly constrained. Our study has only five GRBs in common with AS07. The TAROT study completes what was done by AS07 with a more homogeneous data set. However, the small TAROT aperture induces a brighter cut-off of the distribution.

Figure 6 compares the cumulative distributions of AS07 (AS) and TAROT (TA) at 1000 sec. The most optimistic cases (AS<sub>+</sub> and TA<sub>+</sub>) are computed with the assumption that the non-detections are just below the observed limiting magnitude. This is an extreme case but it allows us to place an upper limit on the distribution. The relative position of TA<sub>+</sub> above AS<sub>+</sub> reveals the differences in limiting magnitudes of the two studies. We calculated also the most pessimistic cases (AS<sub>-</sub> and TA<sub>-</sub>) assuming that the non-detections are fainter than the faintest detected afterglow. The TA<sub>-</sub> distribution follows very well the AS<sub>-</sub> one, until R=17.5 where TA<sub>-</sub> becomes almost flat. One can notice that AS<sub>-</sub> also becomes also flat for R > 20. These two magnitudes corresponds to the typical limiting magnitudes of TAROT and UVOT respectively. The actual distribution must lie between the two + and - curves. AS07 used a recursive method to correct the AS<sub>-</sub> data in order to get the figure 4 of their paper. However, their Figure 4 curve is very close to AS<sub>-</sub>.

The TAROT study confirms the apparent brightness distribution obtained by AS07 for R < 17.5, minimizing the telescope bias. We can see that the proportion of afterglows brighter than R = 14 at 1000 sec is very small (a few percent at most). The slope of the distribution increases slowly until R = 20. The flatness of AS<sub>-</sub> and TA<sub>-</sub> curves may be due to instrumental limitations (i.e. the limiting magnitude) but it can also be the result of the high redshift GRBs ( $z > 5$ ) that are no longer detectable in the R band or by dark GRBs embedded in a dust cocoon that extincts optical wavelengths. Anyway, TAROT confirms that at least 10% of the afterglows are brighter than R = 16.5, 1000 sec after the trigger.

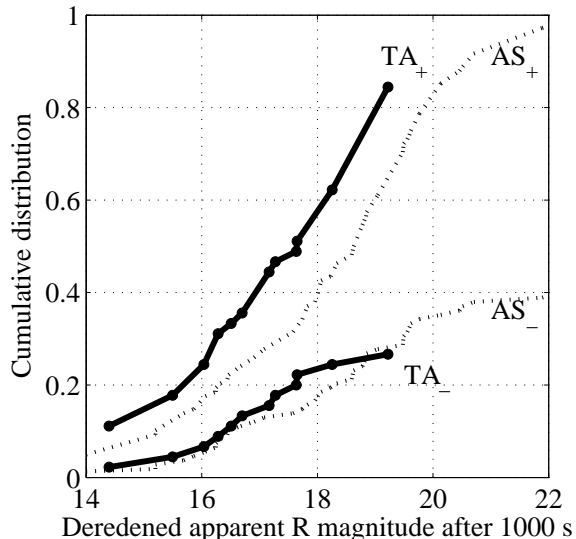


Fig. 6.— Apparent optical brightness distribution of afterglows detected 1000 sec after the GRB. The upper thick line (TA<sub>+</sub>) is constructed assuming that undetected afterglows are just below (*i.e.*, dimmer than) the limiting magnitude. It corresponds to the upper value of the actual distribution (optimistic case in brightness). The lower thick line (TA<sub>-</sub>) is constructed considering all afterglows which are not detected are fainter than the faintest detected afterglow. Dashed lines (AS<sub>-</sub> and AS<sub>+</sub>) are the same limits computed from Tables 1 & 2 of Akerlof & Swan (2007).

## 6. Rising afterglows as standard candles ?

Early GRB afterglows can shine orders of magnitudes brighter than quasars, enabling them to be seen across the entire Universe and opening the possibility to use them to study the geometry of the Universe. However, using GRBs to probe the cosmology can be powerful only if some of their properties are constant and independent from burst to burst. Panaitescu & Vestrand (2008, hereafter PV08) used 11 fast rising afterglows to derive a relation between  $t_p$ , the time of their peak brightness and  $F_p$ , the brightness at their peak (in the GRB rest-frame). Figure 7 displays the optical light-curves observed by TAROT, for GRBs having a spectroscopic redshift or a pseudo-redshift (e.g. Atteia 2005). The axes of Figure 7 are the same as those of Figure 2 of PV08 and the dash-dot line is the PV08  $t_p - F_p$  rela-

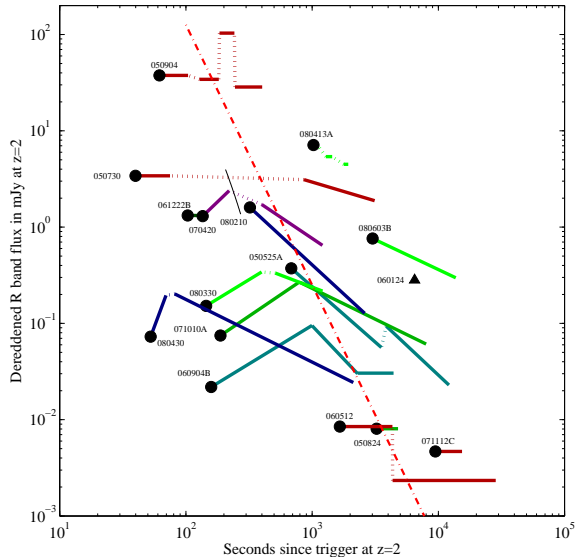


Fig. 7.— Light-curves of afterglows with known redshifts or pseudo-redshifts, placed at a common redshift of  $z=2$ . The dash-dot line is defined as the best correlation between peak times and fluxes for eleven fast rising afterglows (Panaitescu & Vestrand 2008). The peak of the emission of slow rising afterglows appear less correlated with the maximum of the flux than in PV08. This figure appears in colors in the electronic version of this paper.

tion. We used a flat cosmology with  $\Omega_m = 0.27$ ,  $\Omega_\Lambda = 0.73$ , and  $h_0 = 0.71$  to scale fluxes at  $z=2$ . TAROT observations of GRB 050904 and GRB 060904B have been used by PV08 in their study. GRB 060904B and GRB 071010A lie just below the PV08 relation. There is only a pseudo redshift for GRB 070420. The black line passing through the light-curve of GRB 070420 indicates the confidence region of the location of the maximum of brightness.

It must be mentioned that GRB 060904B, GRB 070420, GRB 071010A and GRB 080330 are slow rising afterglows according to the definition of PV08. These afterglows have fainter fluxes in comparison to the PV08  $t_p - F_p$  relation. GRB 080430 is clearly in the category of fast rising afterglows but is very far from the PV08  $t_p - F_p$  relation. At present, the large dispersion of these values does not allow us to consider slow rising

afterglows as useful candles for cosmology. The case of GRB 080430 may indicate that the PV08  $t_p - F_p$  relation is not valid for faint fast rising afterglows (say  $< 1$  mJy at  $z=2$ ).

## 7. Conclusion

Despite its small aperture, TAROT participates actively in the observation of the early optical emission of GRBs. A few GRBs have allowed TAROT to make original contributions to the field of GRB studies: GRB 050904 (optical emission during the prompt at  $z=6.3$ ), GRB 060111B (time-resolved optical emission during the prompt phase), GRB 060904B, GRB 070420, GRB 071010A, GRB 080330 and GRB 080430 (five rising afterglows). We argue that more than half of GRBs have an early optical emission which is fainter than  $R=15.5$  when the gamma emission is still active and we find that only 5 to 20% of the bursts produce a bright optical flash, confirming UVOT observations (Roming et al. 2006). However, these rare bursts are especially interesting and spectacular when they are detected (e.g. GRB 060111B and the recent detection of the optical flash associated with GRB 080319B (Cwiok et al. 2008)). The slope of the afterglow apparent brightness distribution provides new observational data that can be explained by the conjunction of intrinsic parameters (the GRB luminosity function), and extrinsic parameters (the redshift distribution of GRBs). We confirm the result of AS07 that 90% of the afterglows are fainter than  $R=16.5$ , 1000sec after the trigger. We show that a significant fraction of afterglows display an increase in brightness during the first few hundreds of seconds after the trigger. These statistical results enable us to size the next generation of robotic observatories (see AS07 for a discussion). They will feature 1-meter class telescopes and near infrared detectors. Prototypes of these evolutions are REM (Conconi et al. 2004), BOOTES-IR (Castro-Tirado et al. 2005), PAIR-TEL (Bloom 2006), while GROND (Greiner et al. 2008) already represents the new generation of powerful facilities dedicated to the follow-up of GRB early afterglows. Finally, the bulk of the results presented in this paper rest on the large number of GRB localizations provided by *Swift* and on the flawless operation of the TAROT robotic observatories. These conditions will continue to

be realized in the near future with the expectation, thus, of many more interesting discoveries in the coming years.

Acknowledgments: The TAROT telescope has been funded by the *Centre National de la Recherche Scientifique* (CNRS), *Institut National des Sciences de l'Univers* (INSU) and the Carlsberg Foundation. It has been built with the support of the *Division Technique* of INSU. We thank the technical staff contributing to the TAROT project: A. Abchiche, G. Buchholtz, A. Laloge, A. Mayet, M. Merzougui, A.M. Moly, S. Peruchot, H. Pinna, C. Pollas, P. & Y. Richaud, F. Vachier, A. le Van Suu. Bruce Gendre acknowledges a post-doctoral grant funded by the Centre National d'Etudes Spatiales. We thank Alan Imerito for interesting comments on the paper.

## REFERENCES

- Akerlof, C., et al., 1999, *Nature*, 398, 400
- Akerlof, C.W & Swan, H.F, 2007, *ApJ*, 671, 1868
- Atteia, J.-L., 2005 *Il Nuovo Cimento C*, 28, 647
- Barthelmy, S.D., Butterworth, P.S., Cline, T.L., et al., in *AIP Conf. Proc.* 428, *Gamma-Ray bursts*, 1998, ed. C. Meegan & R. Preece (Berlin: Springer), 99
- Berger, E., Kulkarni, S. R., Fox, D. B., 2005, *ApJ*, 634, 501
- Bloom, J.S., Starr, D.L., Blake, C.H., et al., 2006, *Astronomical Data Analysis Software and Systems XV ASP Conference Series*, 351, 751
- Boër, M., Atteia, J.L, Bringer, et al. 2001, *A&A*, 378, 76
- Boër, M., Atteia, J.L., Damerджи, Y., et al. 2006, *ApJ*, 638, L71
- Castro-Tirado, A.J., de Ugarte Postigo, A., Jelnek, M. et al., 2005, *Il Nuovo Cimento C*, 28, 719
- Cwiok, M., Dominik, W., Kasprowicz, G., et al., 2008, *GCNC* 7439
- Conconi, P., Cunniffe, R., D'Alessio, F., et al., 2004, *Proceedings of SPIE*, 5492, 1602
- Fiore, F., Guetta, D., Piranomonte, S., et al., 2006, *Il Nuovo Cimento*, 121, 1935
- Fishman et al., 1992, *como.work*, 26
- Gehrels, N., Chincarini, G., Giommi, P., et al., 2004, *ApJ*, 611, 1005
- Genet, F., Daigne, F., Mochkovitch, R., 2007 *A&A* 471, 1
- Greiner, J., Bornemann, W., Clemens, C., et al., 2008, *PASP* 120, 405
- Jin, Z.P. & Fan, Y.Z., 2007, *MNRAS*, 378, 1043
- Klotz, A., Boër, M., Atteia, J.L., 2003, *A&A* 404, 815
- Klotz, A., Boër, M., Atteia, J.L., et al., 2005, *A&A* 439, L35
- Klotz, A., Boër, M., Atteia, J.L., et al., 2006, *A&A* 451, L39
- Klotz, A., Gendre, B., Stratta, G., et al., 2008, *A&A* 483, 847
- Klotz, A., Boër, M., Eysseric, J., et al., 2008, *PASP* in press
- Panaiteescu, A., & Vestrand, W.T., 2008, *MNRAS*, 387, 497
- Ricker, G., Hurley, K., Lamb, D., 2001, *ApJ* 571, L127
- Roming, P. W. A., et al. 2006, *ApJ*, 652, 1416
- van Paradijs, J., Groot, P. J., Galama, T., et al., 1997, *Nature*, 386, 686
- Vestrand, W. T., Wren, J. A., Wozniak, P. R., 2006, *Nature*, 442, 172
- Zeh, A., Klose, S., & Kann, D. A., 2006, *ApJ*, 637, 889

Table 1: TAROT measurements of GRB optical transients between 2001–2004. Timings are calculated from the GRB trigger. An asterisk (\*) indicates that the measurement was done when the GRB was still active. CR magnitude means Clear filter calibrated with R magnitudes of USNO-B1 stars.

GRB	Trigger	T <sub>90</sub>	TAROT start - end	Magnitude	Reference	Redshift	A <sub>R</sub>
010213	HETE	30s	37.2 - 37.4 h	CR>17	GCNC 936		0.09
020531	HETE	<1s	1.47 - 1.57 h	CR>18.5	Klotz et al. (2003)		0.31
030115	HETE	20s	1.21 - 1.56 h	BR>19.1	GCNC 1810	2.20	0.05
030324	HETE	8.7s	27.9 - 57.9 s	CR>14.8	GCNC 1961		0.07
030329	HETE	25s	6.37 - 6.37 day	CR=18.55 ± 0.36	GCNC 2247	0.16854	0.07
			10.3 - 10.3 day	CR=18.81 ± 0.44	GCNC 2247	0.16854	0.07
030501	INTEGRAL	40s	20 - 50 s*	CR>15	This study		39.55
			20 - 1020 s	CR>18	GCNC 2224		39.55
040916	HETE	450s	2.39 - 2.89 h	CR>19.4	GCNC 2729		0.16
041006	HETE	20s	7.02 - 8.18 h	CR>19.4	GCNC 2784	0.716	0.06
041218	INTEGRAL	60s	1.43 - 3.06 h	CR=19.4 ± 0.2	GCNC 2904		1.68
041219A	INTEGRAL	520s	2.6 - 11.2 min*	CR>18.5	GCNC 2905		4.74

TABLE 2

TAROT MEASUREMENTS OF GRB'S OPTICAL TRANSIENTS IN 2005–2007. DATES ARE CALCULATED FROM THE GRB TRIGGER. AN ASTERISK (\*) INDICATES THAT THE MEASUREMENT WAS DONE WHEN THE GRB WAS STILL ACTIVE. THE RIGHT ARROW SYMBOL ( $\rightarrow$ ) DESIGNATES A SERIES OF MEASUREMENTS WITH THE MAGNITUDE BEING THAT AT THE STARTING TIME FOLLOWED BY TEMPORAL DECAY ACCORDING TO THE  $f(t) \propto t^{-\alpha}$  LAW. REDSHIFT WRITTEN IN ITALIC MEANS THAT THEY ARE PSEUDO-REDSHIFTS (ATTEIA 2005). SITE OF OBSERVATION IS CALERN OBSERVATORY (C) OR LA SILLA OBSERVATORY (S). CR MAGNITUDE MEANS CLEAR FILTER CALIBRATED WITH R MAGNITUDES OF USNO-B1 STARS. CI MEANS CLEAR FILTER CALIBRATED WITH I MAGNITUDES. NOTE THAT ALL MAGNITUDES DISPLAYED ARE NOT CORRECTED FOR GALACTIC EXTINCTION.

GRB	Trigger	T <sub>90</sub>	TAROT start - end	Magnitude	Reference	Site	Redshift	A <sub>R</sub>
050209	HETE	40s	2.40 - 3.22 h	CR>19.2	GCNC 3020	c	<i>2.93 ± 1.6</i>	0.11
050306	SWIFT	180s	126 - 157 s*	CR>11	GCNC 3084	c		1.814
			210 - 440 s	CR>13	GCNC 3084	c		1.814
			505 - 619 s	CR>14.0	GCNC 3084	c		1.814
			45 - 80 min	CR>17.5	GCNC 3084	c		1.814
050408	HETE	34s	3.48 - 3.84 h	CR>18.7	This study	c	1.2357	0.07
050416	SWIFT	2.4s	8.40 - 9.52 h	CR>18.4	This study	c	0.6535	0.08
050504	INTEGRAL	80s	12.11 - 12.15 h	CR>17.5	This study	c		0.03
050505	SWIFT	63s	9.46 - 17.06 min	CI=18.2 ± 0.2	GCNC 3403	c	4.27	0.06
			17.18 - 24.78 min	CI=18.4 ± 0.2	GCNC 3403	c	4.27	0.06
			27.57 - 37.30 min	CI>18.8	GCNC 3403	c	4.27	0.06
050520	INTEGRAL	20s	37 - 52 s	CR>16.0	This study	c		0.04
			59 - 74 s	CR>16.0	This study	c		0.04
			80 - 441 s	CR>17.2	This study	c		0.04
050525A	SWIFT	8.8s	6.1 → 31.6 min	CR=14.5 α=1.15	Klotz et al. (2005)	c	0.606	0.26
			34.5 → 108.3 min	CR=16.0 α=1.23	Klotz et al. (2005)	c	0.606	0.26
050730	SWIFT	35s	66 - 124 s	CR=16.7 ± 0.4	GCNC 3720	c	3.967	0.14
			23.8 → 86.4 min	CR=16.8 α=0.39	This study	c	3.967	0.14
050803	SWIFT	110s	61 - 63 min	CR>16.0	GCNC 3751	c		0.20
			84 - 156 min	CR>18.7	GCNC 3751	c		0.20
050824	SWIFT	70s	9.8 - 10.1 min	CR>16.4	This study	c	0.83	0.09
			33.0 - 48.8 min	CR=19.3 ± 0.4	This study	c	0.83	0.09
050904	SWIFT	225s	86 - 144 s*	CI>15.3	Boër et al. (2006)	c	6.29	0.17
			150 - 253 s*	CI=15.2 ± 0.3	Boër et al. (2006)	c	6.29	0.17
			312 - 443 s	CI=15.3 ± 0.3	Boër et al. (2006)	c	6.29	0.17
			449 - 589 s	CI=14.1 ± 0.3	Boër et al. (2006)	c	6.29	0.17
			595 - 978 s	CI≈15.5 ± 0.4	Boër et al. (2006)	c	6.29	0.17
			985 - 1666 s	CI>15.8	Boër et al. (2006)	c	6.29	0.17
051211A	HETE	<1s	3.14 - 3.19 h	CR>15.3	GCNC 4329	c	<i>4.9 ± 2.0</i>	0.32
051211B	INTEGRAL	80s	131 - 161 s	CR>16.2	GCNC 4328	c		1.25
051221B	SWIFT	192s	216 → 276 s	CR>14	GCNC 4386	c		3.71
			282 - 312 s	CR>18.2	GCNC 4386	c		3.71
060111A	SWIFT	20s	20 → 80 s	CR>16.2	GCNC 4483	c		0.08
			86 - 261 s	CR=18.3 ± 0.4	GCNC 4483	c		0.08
			510 - 1027 s	CR>18.7	GCNC 4483	c		0.08
060111B	SWIFT	59s	28 → 88 s*	CR=13.8 α=2.38	Klotz et al. (2006)	c		0.30
			94 → 198 s	CR=16.75 α=1.08	Klotz et al. (2006)	c		0.30
060124	SWIFT	710s	1.98 - 2.71 h	CR<18.3	This study	c	2.297	0.36
060502B	SWIFT	<1s	2.08 - 2.60 h	CR>16.8	This study	c	0.287?	0.12
060512	SWIFT	8.6s	13.3 - 34.7 min	CR=17.6 ± 0.3	GCNC 5140	c	0.4428	0.05
			34.8 - 228.3 min	CR=19.0 ± 0.6	GCNC 5140	c	0.4428	0.05
060515	SWIFT	52s	60 → 120 s	CR>15.1	GCNC 5134	c		0.08
			126 - 156 s	CR>16.2	GCNC 5134	c		0.08
			2.1 - 25.0 min	CR>18.2	GCNC 5134	c		0.08
060712	SWIFT	26s	104 → 164 s	CR>12.5	This study	c		0.03
			171 - 458 s	CR>13.8	This study	c		0.03
060814	SWIFT	140s	21 → 81 s*	CR>14.8	GCNC 5448	c	0.84	0.11
			88 - 118 s*	CR>15.7	GCNC 5448	c	0.84	0.11
			125 - 155 s*	CR>15.7	GCNC 5448	c	0.84	0.11
			161 - 191 s	CR>15.7	GCNC 5448	c	0.84	0.11

TABLE 2—Continued

GRB	Trigger	T <sub>90</sub>	TAROT start - end	Magnitude	Reference	Site	Redshift	A <sub>R</sub>
060904A	SWIFT	80s	88 - 228 s	CR>17.4	GCNC 5448	c	0.84	0.11
			27 → 87 s*	CR>16.0	GCNC 5506	c	$1.84 \pm 0.85$	0.05
			94 - 124 s	CR>17.3	GCNC 5506	c	$1.84 \pm 0.85$	0.05
			94 - 376 s	CR>19.5	GCNC 5506	c	$1.84 \pm 0.85$	0.05
060904B	SWIFT	192s	23 → 41 s*	CR>17.2	Klotz et al. (2008)	c	0.703	0.46
			41 → 44 s*	CR>15.9	Klotz et al. (2008)	c	0.703	0.46
			44 → 86 s*	CR>17.2	Klotz et al. (2008)	c	0.703	0.46
			1.50 → 9.45 min*	CR=18.16 α=-0.80	Klotz et al. (2008)	c	0.703	0.46
			9.45 → 21.7 min	CR=16.57 α=1.38	Klotz et al. (2008)	c	0.703	0.46
			21.7 → 41.8 min	CR=17.8 ± 0.1 α=0	Klotz et al. (2008)	c	0.703	0.46
060919	SWIFT	9s	28 → 88 s	CR>15.4	GCNC 5576	s		0.19
			94 - 124 s	CR>15.8	GCNC 5576	s		0.19
			94 - 196 s	CR>15.9	GCNC 5576	s		0.19
061019	SWIFT	191s	15.0 - 16.5 min	CR>14.8	GCNC 5731	s		3.01
			15.0 - 23.2 min	CR>15.8	GCNC 5731	s		3.01
061027	SWIFT	170s	14.0 - 18.6 h	R>20.0	GCNC 5788	s		0.41
061028	SWIFT	106s	14.0 - 18.6 h	I>18.9	GCNC 5788	s		0.41
			145 → 205 s	CR>16.5	GCNC 5763	c		0.42
			212 - 242 s	CR>17.5	GCNC 5763	c		0.42
			212 - 497 s	CR>18.3	GCNC 5763	c		0.42
061110B	SWIFT	128s	0.44 - 1.07 h	CR>20.1	GCNC 5764	c		0.42
			10.4 - 11.9 min	CR>16.6	GCNC 5801	c	3.44	0.11
			10.4 - 18.3 min	CR>16.9	GCNC 5801	c	3.44	0.11
061217	SWIFT	0.3s	20.2 → 80.2 s	CR>16.5	GCNC 5942	c	0.827	0.12
			87 - 117 s	CR>18.1	GCNC 5942	c	0.827	0.12
061218	SWIFT	4s	87 - 371 s	CR>19.2	GCNC 5942	c	0.827	0.12
			61 → 121 s	CR>15.8	GCNC 5980	s		0.34
			127 - 157 s	CR>17.4	GCNC 5943	s		0.34
			162 - 192 s	CR>17.4	GCNC 5943	s		0.34
061222B	SWIFT	40s	127 - 511 s	CR>18.0	GCNC 5943	s		0.34
			84 → 108 s	CR>17.7	GCNC 5981	s	3.355	1.01
			108 → 144 s	CR>14.7	GCNC 5981	s	3.355	1.01
			150 - 180 s	CR=18.2 ± 0.5	GCNC 5960	s	3.355	1.01
			185 - 215 s	CR>18.2	GCNC 5981	s	3.355	1.01
070103	SWIFT	19s	150 - 534 s	CR>19.9	GCNC 5959	s	3.355	1.01
			23 → 83 s	CR>15.1	GCNC 5989	c		0.18
			89 - 120 s	CR>15.9	GCNC 5989	c		0.18
			89 - 229 s	CR>16.4	GCNC 5989	c		0.18
070227	SWIFT	7s	7.8 - 9.0 h	CR>20.2	GCNC 6159	s		0.90
070330	SWIFT	9s	2.5 - 3.5 h	CR>17.4	GCNC 6235	s		0.17
070411	SWIFT	101s	46 → 106 s*	CR>14.6	GCNC 6487	c	2.954	0.76
			113 - 143 s	CR>15.5	GCNC 6487	c	2.954	0.76
070412	SWIFT	34s	11.3 - 12.8 min	CR>18.5	GCNC 6488	c		0.06
			11.3 - 20.9 min	CR>19.5	GCNC 6488	c		0.06
070420	SWIFT	77s	40 → 49 s*	CR>16.75	Klotz et al. (2008)	s	$1.56 \pm 0.35$	1.39
			49 → 57 s*	CR>16.45	Klotz et al. (2008)	s	$1.56 \pm 0.35$	1.39
			57 → 66 s*	CR>16.25	Klotz et al. (2008)	s	$1.56 \pm 0.35$	1.39
			66 → 91 s*	CR>16.75	Klotz et al. (2008)	s	$1.56 \pm 0.35$	1.39
			116 → 188 s	CR=16.7 α=-1.26	Klotz et al. (2008)	s	$1.56 \pm 0.35$	1.39
			341 → 1031 s	CR=16.4 α=0.88	Klotz et al. (2008)	s	$1.56 \pm 0.35$	1.39

TABLE 2—Continued

GRB	Trigger	T <sub>90</sub>	TAROT start - end	Magnitude	Reference	Site	Redshift	A <sub>R</sub>
070508	SWIFT	40s	13.8 - 15.3 min	CR>17.8	GCNC 6384	s		0.37
			13.8 - 28.4 min	CR>19.7	GCNC 6384	s		0.37
070521	SWIFT	38s	24 → 84 s*	CR>17.1	GCNC 6434	s	2.28 ± 0.45	0.07
			89 - 119 s	CR>17.5	GCNC 6434	s	2.28 ± 0.45	0.07
			89 - 570 s	CR>19.0	GCNC 6434	s	2.28 ± 0.45	0.07
070621	SWIFT	33s	23 → 83 s*	CR>14.9	GCNC 6563	c		0.13
			90 - 120 s	CR>15.4	GCNC 6563	c		0.13
070628	SWIFT	39s	8.3 - 9.1 h	CR>17.9	GCNC 6588	s		2.42
070913	SWIFT	8s	87 - 117 s	CR=17.5 ± 0.5	GCNC 6787	s		0.35
			124 - 154 s	CR=18 ± 0.5	GCNC 6787	s		0.35
			288 - 378 s	CR>18	GCNC 6787	s		0.35
070920A	SWIFT	56s	9.1 - 10.6 min	CR>18.2	GCNC 6806	c		0.29
070920B	SWIFT	20s	2.7 - 3.6 h	CR>18.2	GCNC 6816	s		0.04
071010A	SWIFT	6s	124 → 514 s	CR=17.5 α=-0.89	This study	s	0.98	0.28
			8.8 → 88 min	CR=16.12 α=0.64	This study	s	0.98	0.28
071101	SWIFT	3s	39 → 99 s	CR>16.3	GCNC 7035	c		3.99
			106 - 136 s	CR>17.5	GCNC 7035	c		3.99
			106 - 394 s	CR>18.4	GCNC 7035	c		3.99
071109	INTEGRAL	30s	36 - 96 s	CR>15.4	GCNC 7052	c		1.74
			103 - 133 s	CR>15.5	GCNC 7052	c		1.74
071112B	SWIFT	0.30s	5.8 - 10.5 h	R>20.4	This study	s		0.56
071112C	SWIFT	15s	1.6 - 2.6 h	CR=20.1	GCNC 7065	c	0.8230	0.32
071117	SWIFT	6.6s	9.5 - 11.3 h	CI>20	GCNC 7108	s		0.06
080129	SWIFT	80s	59 - 74 min	CR>16.4	GCNC 7234	s		2.724
080207	SWIFT	300s	26 - 27 min	CR>14.3	GCNC 7267	c		0.062
080210	SWIFT	45s	390 → 3162 s	CR=16.62 α=1.21	This study	s	2.64	0.223
080315	SWIFT	45s	85 - 91 s	CR>16.8	GCNC 7417	c		0.036
080330	SWIFT	61s	20.4 → 80.4 s	CR>16.6	This study	c	1.51	0.044
			121 → 333 s	CR=17.6 α=-0.8	This study	c	1.51	0.044
			428 → 1012 s	CR=16.75 α=0.5	This study	c	1.51	0.044
080413A	SWIFT	46s	480 - 520 s	CR>12.5	GCNC 7595	c	2.433	0.423
			1174 - 1263 s	CR=15.0 ± 0.2	GCNC 7595	c	2.433	0.423
			1470 - 1650 s	CR=15.3 ± 0.2	GCNC 7595	c	2.433	0.423
			2035 - 2215 s	CR=15.5 ± 0.2	GCNC 7595	c	2.433	0.423
080430	SWIFT	16s	18.8 → 25.2 s*	CR>16.7	This study	c	0.767	0.033
			31 → 41 s	CR=16.65 α=-3.53	This study	c	0.767	0.033
			48 → 1250 s	CR=15.54 α=0.65	This study	c	0.767	0.033
080516	SWIFT	5.8s	65 → 124 s	CR>13.5	GCNC 7798	s	3.2 ± 0.3	1.1
			131 - 161 s	CR>15	GCNC 7798	s	3.2 ± 0.3	1.1
080603B	SWIFT	70s	1.03 → 4.7 h	CR=17.3 α=0.62	This study	c	2.69	0.05
080903	SWIFT	66s	29.1 → 89.1 s*	CR>17.1	This study	c		0.556
			96 - 126 s	CR>18.2	This study	c		0.556